











TECH BRIEFS

NATIONAL AERONAUTICS AND SPACE ADMINISTRATION

-  **Technology Focus**
-  **Electronics/Computers**
-  **Software**
-  **Materials**
-  **Mechanics/Machinery**
-  **Manufacturing**
-  **Bio-Medical**
-  **Physical Sciences**
-  **Information Sciences**
-  **Books and Reports**

INTRODUCTION

Tech Briefs are short announcements of innovations originating from research and development activities of the National Aeronautics and Space Administration. They emphasize information considered likely to be transferable across industrial, regional, or disciplinary lines and are issued to encourage commercial application.

Additional Information on NASA Tech Briefs and TSPs

Additional information announced herein may be obtained from the NASA Technical Reports Server: <http://ntrs.nasa.gov>.

Please reference the control numbers appearing at the end of each Tech Brief. Information on NASA's Innovative Partnerships Program (IPP), its documents, and services is available on the World Wide Web at <http://www.ipp.nasa.gov>.

Innovative Partnerships Offices are located at NASA field centers to provide technology-transfer access to industrial users. Inquiries can be made by contacting NASA field centers listed below.

NASA Field Centers and Program Offices

Ames Research Center

Mary Walsh
(650) 604-1405
mary.w.walsh@nasa.gov

Dryden Flight Research Center

Ron Young
(661) 276-3741
ronald.m.young@nasa.gov

Glenn Research Center

Joe Shaw
(216) 977-7135
robert.j.shaw@nasa.gov

Goddard Space Flight Center

Nona Cheeks
(301) 286-5810
nona.k.cheeks@nasa.gov

Jet Propulsion Laboratory

Indrani Graczyk
(818) 354-2241
indrani.graczyk@jpl.nasa.gov

Johnson Space Center

John E. James
(281) 483-3809
john.e.james@nasa.gov

Kennedy Space Center

David R. Makufka
(321) 867-6227
david.r.makufka@nasa.gov

Langley Research Center

Michelle Ferebee
(757) 864-5617
michelle.t.ferebee@nasa.gov

Marshall Space Flight Center

Jim Dowdy
(256) 544-7604
jim.dowdy@nasa.gov

Stennis Space Center

Ramona Travis
(228) 688-3832
ramona.e.travis@ssc.nasa.gov

NASA Headquarters

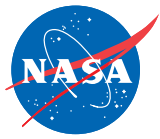
Innovative Partnerships Office

Doug Comstock, Director
(202) 358-2221
doug.comstock@nasa.gov

Daniel Lockney,
Technology Transfer Lead
(202) 358-2037
daniel.p.lockney@nasa.gov

Small Business Innovation Research (SBIR) & Small Business Technology Transfer (STTR) Programs

Carl Ray, Program Executive
(202) 358-4652
carl.g.ray@nasa.gov



TECH BRIEFS

NATIONAL AERONAUTICS AND SPACE ADMINISTRATION

5 Technology Focus: Sensors

- 5 Laser Truss Sensor for Segmented Telescope Phasing
- 5 Qualifications of Bonding Process of Temperature Sensors to Deep-Space Missions
- 5 Optical Sensors for Monitoring Gamma and Neutron Radiation
- 6 Compliant Tactile Sensors
- 6 Cytometer on a Chip

9 Electronics/Computers

- 9 Measuring Input Thresholds on an Existing Board
- 9 Scanning and Defocusing Properties of Microstrip Reflectarray Antennas
- 10 Cable Tester Box
- 10 Programmable Oscillator
- 10 Fault-Tolerant, Radiation-Hard DSP
- 11 Sub-Shot Noise Power Source for Microelectronics

13 Software

- 13 Asynchronous Message Service Reference Implementation
- 13 Zero-Copy Objects System
- 13 Delay and Disruption Tolerant Networking MACHETE Model
- 14 Contact Graph Routing
- 14 Parallel Eclipse Project Checkout

17 Manufacturing & Prototyping

- 17 Technique for Configuring an Actively Cooled Thermal Shield in a Flight System

19 Materials & Coatings

- 19 Use of Additives to Improve Performance of Methyl Butyrate-Based Lithium-Ion Electrolytes

- 19 Li-Ion Cells Employing Electrolytes With Methyl Propionate and Ethyl Butyrate Co-Solvents

21 Bio-Medical

- 21 Improved Devices for Collecting Sweat for Chemical Analysis
- 21 Tissue Photolithography
- 22 Method for Impeding Degradation of Porous Silicon Structures
- 22 External Cooling Coupled to Reduced Extremity Pressure Device

25 Physical Sciences

- 25 A Zero-Gravity Cup for Drinking Beverages in Microgravity
- 26 Co-Flow Hollow Cathode Technology
- 26 Programmable Aperture With MEMS Microshutter Arrays
- 27 Polished Panel Optical Receiver for Simultaneous RF/Optical Telemetry With Large DSN Antennas

29 Information Sciences

- 29 Adaptive System Modeling for Spacecraft Simulation
- 29 Lidar-Based Navigation Algorithm for Safe Lunar Landing
- 30 Tracking Object Existence From an Autonomous Patrol Vehicle

31 Books & Reports

- 31 Rad-Hard, Miniaturized, Scalable, High-Voltage Switching Module for Power Applications
- 31 Architecture for a 1-GHz Digital RADAR

This document was prepared under the sponsorship of the National Aeronautics and Space Administration. Neither the United States Government nor any person acting on behalf of the United States Government assumes any liability resulting from the use of the information contained in this document, or warrants that such use will be free from privately owned rights.



Laser Truss Sensor for Segmented Telescope Phasing

NASA's Jet Propulsion Laboratory, Pasadena, California

A paper describes the laser truss sensor (LTS) for detecting piston motion between two adjacent telescope segment edges. LTS is formed by two point-to-point laser metrology gauges in a crossed geometry.

A high-resolution (<30 nm) LTS can be implemented with existing laser metrology gauges. The distance change between the reference plane and the target plane is measured as a function of the phase change between the reference and target beams. To ease the bandwidth require-

ments for phase detection electronics (or phase meter), homodyne or heterodyne detection techniques have been used.

The phase of the target beam also changes with the refractive index of air, which changes with the air pressure, temperature, and humidity. This error can be minimized by enclosing the metrology beams in baffles. For longer-term (weeks) tracking at the micron level accuracy, the same gauge can be operated in the absolute metrology mode with an accuracy of microns; to implement ab-

solute metrology, two laser frequencies will be used on the same gauge. Absolute metrology using heterodyne laser gauges is a demonstrated technology. Complexity of laser source fiber distribution can be optimized using the range-gated metrology (RGM) approach.

This work was done by Duncan T. Liu, Oliver P. Lay, Alireza Azizi, Herman Erlig, Leonard I. Dorsky, Cheryl G. Asbury, and Feng Zhao of Caltech for NASA's Jet Propulsion Laboratory. Further information is contained in a TSP (see page 1). NPO-47753

Qualifications of Bonding Process of Temperature Sensors to Deep-Space Missions

NASA's Jet Propulsion Laboratory, Pasadena, California

A process has been examined for bonding a platinum resistance thermometer (PRT) onto potential aerospace materials such as flat aluminum surfaces and a flexible copper tube to simulate coaxial cables for flight applications. Primarily, PRTs were inserted into a silver-plated copper braid to avoid stresses on the sensor while the sensor was attached with the braid to the base material for long-duration, deep-space missions.

Al-1145/graphite composite (planar substrate) and copper tube have been used in this study to assess the reliability of PRT bonding materials. A flexible copper tube was chosen to simulate the coaxial cable to attach PRTs. The sub-

strate materials were cleaned with acetone wipes to remove oils and contaminants. Later, the surface was also cleaned with ethyl alcohol and was air-dried. The materials were gently abraded and then were cleaned again the same way as previously mentioned.

Initially, shielded (silver plated copper braid) PRT (type X) test articles were fabricated and cleaned. The base antenna material was pretreated and shielded, and CV-2566 NuSil silicone was used to attach the shielded PRT to the base material. The test articles were cured at room temperature and humidity for seven days. The resistance of the PRTs was continuously monitored dur-

ing the thermal cycling, and the test articles were inspected prior to, at various intermediate steps during, and at the end of the thermal cycling as well. All of the PRTs survived three times the expected mission life for the JUNO project. No adhesion problems were observed in the PRT sensor area, or under the shielded PRT. Furthermore, the PRT resistance accurately tracked the thermal cycling of the chamber.

This work was done by Rajeshuni Ramesham, Amarit Kitiyakara, Richard W. Redick III, and Eric T. Sunada of Caltech for NASA's Jet Propulsion Laboratory. For more information, contact iaoffice@jpl.nasa.gov. NPO-47682

Optical Sensors for Monitoring Gamma and Neutron Radiation

John H. Glenn Research Center, Cleveland, Ohio

For safety and efficiency, nuclear reactors must be carefully monitored to provide feedback that enables the fission rate to be held at a constant target level via adjustments in the position of neutron-absorbing rods and moderating coolant flow rates. For automated reactor control, the monitoring system

should provide calibrated analog or digital output. The sensors must survive and produce reliable output with minimal drift for at least one to two years, for replacement only during refueling. Small sensor size is preferred to enable more sensors to be placed in the core for more detailed characterization of

the local fission rate and fuel consumption, since local deviations from the norm tend to amplify themselves. Currently, reactors are monitored by local power range meters (LPRMs) based on the neutron flux or gamma thermometers based on the gamma flux. LPRMs tend to be bulky, while gamma ther-

ometers are subject to unwanted drift. Both electronic reactor sensors are plagued by electrical noise induced by ionizing radiation near the reactor core.

A fiber optic sensor system was developed that is capable of tracking thermal neutron fluence and gamma flux in order to monitor nuclear reactor fission rates. The system provides near-real-time feedback from small-profile probes that are not sensitive to electromagnetic noise.

The key novel feature is the practical design of fiber optic radiation sensors. The use of an actinoid element to monitor neutron flux in fiber optic EFPI (extrinsic Fabry-Perot interferometric) sensors is a new use of material. The materials and structure used in the sensor construction can be adjusted to result in a sensor that is sensitive to just thermal, gamma, or neutron stimulus, or any combination of the three. The tested design showed low sensitivity to

thermal and gamma stimuli and high sensitivity to neutrons, with a fast response time.

This work was done by Clark D. Boyd of Luna Innovations, Inc. for Glenn Research Center.

Inquiries concerning rights for the commercial use of this invention should be addressed to NASA Glenn Research Center, Innovative Partnerships Office, Attn: Steven Fedor, Mail Stop 4-8, 21000 Brookpark Road, Cleveland, Ohio 44135. Refer to LEW-18701-1.

Compliant Tactile Sensors

Lyndon B. Johnson Space Center, Houston, Texas

Tactile sensors are currently being designed to sense interactions with human hands or pen-like interfaces. They are generally embedded in screens, keyboards, mousepads, and pushbuttons. However, they are not well fitted to sense interactions with all kinds of objects.

A novel sensor was originally designed to investigate robotics manipulation where not only the contact with an object needs to be detected, but also where the object needs to be held and manipulated. This tactile sensor has been designed with features that allow it to sense a large variety of objects in human environments.

The sensor is capable of detecting forces coming from any direction. As a result, this sensor delivers a force vector with three components. In contrast to most of the tactile sensors that are flat, this one sticks out from the surface so that it is likely to come in contact with

objects. The sensor conforms to the object with which it interacts. This augments the contact's surface, consequently reducing the stress applied to the object. This feature makes the sensor ideal for grabbing objects and other applications that require compliance with objects. The operational range of the sensor allows it to operate well with objects found in peoples' daily life. The fabrication of this sensor is simple and inexpensive because of its compact mechanical configuration and reduced electronics. These features are convenient for mass production of individual sensors as well as dense arrays.

The biologically inspired tactile sensor is sensitive to both normal and lateral forces, providing better feedback to the host robot about the object to be grabbed. It has a high sensitivity, enabling its use in manipulation fingers, which typically have low mechanical impedance in

order to be very compliant. The construction of the sensor is simple, using inexpensive technologies like silicon rubber molding and standard stock electronics.

This work was done by Eduardo R. Torres-Jara of the Massachusetts Institute of Technology for Johnson Space Center. For further information, contact the JSC Innovation Partnerships Office at (281) 483-3809.

In accordance with Public Law 96-517, the contractor has elected to retain title to this invention. Inquiries concerning rights for its commercial use should be addressed to:

*Massachusetts Institute of Technology
Five Cambridge Center*

Kendall Square

Room NE25-230

Cambridge, MA 02142-1493

Phone No.: (617) 253-6966

E-mail: tlo@mit.edu

Refer to MSC-24271-1, volume and number of this NASA Tech Briefs issue, and the page number.

Cytometer on a Chip

Analyses could be performed rapidly in compact instruments using disposable chips.

Lyndon B. Johnson Space Center, Houston, Texas

A cytometer now under development exploits spatial sorting of sampled cells on a microarray chip followed by use of grating-coupled surface-plasmon-resonance imaging (GCSPRI) to detect the sorted cells. This cytometer on a chip is a prototype of contemplated future miniature cytometers that would be suitable for rapidly identifying pathogens and other cells of interest in both field and laboratory applications and that would be attractive as alternatives to conventional flow cytometers.

The basic principle of operation of a conventional flow cytometer requires fluorescent labeling of sampled cells, stringent optical alignment of a laser beam with a narrow orifice, and flow of the cells through the orifice, which is subject to clogging. In contrast, the principle of operation of the present cytometer on a chip does not require fluorescent labeling of cells, stringent optical alignment, or flow through a narrow orifice. The basic principle of operation of

the cytometer on a chip also reduces the complexity, mass, and power of the associated laser and detection systems, relative to those needed in conventional flow cytometry.

Instead of making cells flow in single file through a narrow flow orifice for sequential interrogation as in conventional flow cytometry, a liquid containing suspended sampled cells is made to flow over the front surface of a microarray chip on which there are many cap-

ture spots. Each capture spot is coated with a thin (≈ 50 -nm) layer of gold that is, in turn, coated with antibodies that bind to cell-surface molecules characteristic of one the cell species of interest. The multiplicity of capture spots makes it possible to perform rapid, massively parallel analysis of a large cell population.

The binding of cells to each capture spot gives rise to a minute change in the index of refraction at the surface of the chip. This change in the index of refraction is what is sensed in GCSPRI, as described briefly below. The identities of the various species in a sample of cells is spatially encoded in the chip by the pattern of capture spots. The number of cells of a particular species is determined from the magnitude of the GCSPRI signal from that spot.

GCSPRI as used here can be summarized as follows: The cytometer chip is fabricated with a diffraction grating on its front surface. The chip is illuminated with a light emitting diode (LED) from the front. By proper choice of grating parameters and of the wavelength and

the angle of incidence of a laser beam, laser light can be made to be coupled into an electromagnetic mode that resonates with surface plasmons and thus couples light into surface plasmons. Coupling of light into a surface plasmon at a given location reduces the amount of incident light reflected from that location. A change in the index of refraction at the surface of a capture spot gives rise to a change in the resonance condition. Depending on the specific design, the change in the index of refraction could manifest itself as a brightening or darkening, a change in the wavelength needed to excite the plasmon at a given angle of incidence, or a change in the angle of incidence needed to excite the plasmon at a given wavelength.

Whereas a multiwavelength laser system with multichannel detection would be needed to detect multiple species in conventional flow cytometry, it suffices to use an LED and a single detector channel in the GCSPRI approach: this contributes significantly to reductions in cost, complexity, size, mass, and power. GCSPRI cytometer chips could

be made of plastic and could be mass-produced cheaply by use of molding and other methods adopted from the manufacture of digital video disks. These methods are amenable to a high degree of miniaturization: such additional features as fluidic channels, reaction chambers, and fluid-coupling ports could readily be incorporated into the chips, without incurring substantial additional costs.

This work was done by Salvador M. Fernandez of Ciencia, Inc., for Johnson Space Center. Further information is contained in a TSP (see page 1).

In accordance with Public Law 96-517, the contractor has elected to retain title to this invention. Inquiries concerning rights for its commercial use should be addressed to:

*Dr. Salvador M. Fernandez, President
Ciencia, Inc.*

*111 Roberts Street, Suite K
East Hartford, CT. 06108*

Phone No.:(860) 528-9737

Fax No.:(860) 528-5658

Refer to MSC-23711-1/4224-1, volume and number of this NASA Tech Briefs issue, and the page number.



Measuring Input Thresholds on an Existing Board

NASA's Jet Propulsion Laboratory, Pasadena, California

A critical PECL (positive emitter-coupled logic) interface to Xilinx interface needed to be changed on an existing flight board. The new Xilinx input interface used a CMOS (complementary metal-oxide semiconductor) type of input, and the driver could meet its thresholds typically, but not in worst-case, according to the data sheet. The previous interface had been based on comparison with an external reference, but the CMOS input is based on comparison with an internal divider from the power supply. A way to measure what the exact input threshold was for this device for 64 inputs on a flight board was needed.

The measurement technique allowed an accurate measurement of the voltage required to switch a Xilinx input from high to low for each of the 64 lines, while only probing two of them. Directly driving an external voltage was consid-

ered too risky, and tests done on any other unit could not be used to qualify the flight board. The two lines directly probed gave an absolute voltage threshold calibration, while data collected on the remaining 62 lines without probing gave relative measurements that could be used to identify any outliers.

The PECL interface was forced to a long-period square wave by driving a saturated square wave into the ADC (analog to digital converter). The active pull-down circuit was turned off, causing each line to rise rapidly and fall slowly according to the input's weak pull-down circuitry. The fall time shows up as a change in the pulse width of the signal ready by the Xilinx. This change in pulse width is a function of capacitance, pull-down current, and input threshold. Capacitance was known from the different trace lengths, plus a gate input capaci-

tance, which is the same for all inputs. The pull-down current is the same for all inputs including the two that are probed directly. The data was combined, and the Excel solver tool was used to find input thresholds for the 62 lines. This was repeated over different supply voltages and temperatures to show that the interface had voltage margin under all worst case conditions.

Gate input thresholds are normally measured at the manufacturer when the device is on a chip tester. A key function of this machine was duplicated on an existing flight board with no modifications to the nets to be tested, with the exception of changes in the FPGA program.

This work was done by Igor Kuperman, Daniel G. Gutrich, and Andrew C. Berkun of Caltech for NASA's Jet Propulsion Laboratory. For more information, contact iaoffice@jpl.nasa.gov. NPO-47705

Scanning and Defocusing Properties of Microstrip Reflectarray Antennas

Microstrip reflectarrays have applications in radar and remote sensing systems.

NASA's Jet Propulsion Laboratory, Pasadena, California

A symmetric reflectarray, consisting of variable-size square patch elements with a commonly used mathematical model for the horn in the form of a cosine function, has been designed using the transmit mode technique for different f/D ratios with -10 dB edge taper. Subsequently, the antennas were analyzed for the radiation pattern and gain. The infinite array model was used to determine the reflection phase of each patch element in the design and analysis codes. By displacing the feed laterally, the scan characteristics were obtained, such as the beam deviation factor, gain loss, and pattern degradation. The properties of reflectarrays were compared to those of the conventional paraboloidal reflectors. The same procedure was used to study the scan properties of offset reflectarrays. There is no cross-polarized radiation in the princi-

pal planes for a symmetric system. Cross-polarized radiation exists in non-principal planes off broadside in symmetric systems, with greater levels for larger values of subtended angles. Such cross-polarized radiation level increases with subtended angle just as cross-polarization level increases with decreasing values of f/D ratios for symmetric paraboloids in non-principal planes. Pattern distortions and gain loss were found to be more severe in the case of a microstrip reflectarray compared to the conventional parabolic reflector. The scan performance of the reflectarrays was found to improve with f/D ratios as is true for paraboloids. In general, scanning by means of displaced feed is limited to a few beamwidths in reflectarrays.

Feed displacement in the axial direction of a symmetric reflectarray was in-

vestigated and compared to that of paraboloids. The gain loss due to the defocused feed of a reflectarray was found to be nearly the same as that of a paraboloid of the same subtended angle for larger values of f/D , and for displacements away from the antenna. The gain loss of an axially defocused reflectarray was found to be greater than that of a paraboloid for displacements closer to the antenna, especially for smaller values of f/D .

In general, the performance of a defocused reflectarray was found to be poorer than that of a comparable paraboloid reflector.

This work was done by Sembiam Rengarajan of Caltech for NASA's Jet Propulsion Laboratory. For more information, contact iaoffice@jpl.nasa.gov. NPO-47550

Cable Tester Box

NASA's Jet Propulsion Laboratory, Pasadena, California

Cables are very important electrical devices that carry power and signals across multiple instruments. Any fault in a cable can easily result in a catastrophic outcome. Therefore, verifying that all cables are built to spec is a very important part of Electrical Integration Procedures. Currently, there are two methods used in lab for verifying cable connectivity. (1) Using a Break-Out Box and an ohmmeter — this method is time-consuming but effective for custom cables — and (2) Commercial Automated Cable Tester Boxes — this method is fast, but to test custom cables often requires pre-programmed configuration files, and cables used on spacecraft are often uniquely designed for specific purposes.

The idea is to develop a semi-automatic continuity tester that reduces

human effort in cable testing, speeds up the electrical integration process, and ensures system safety.

The JPL-Cable Tester Box is developed to check every single possible electrical connection in a cable in parallel. This system indicates connectivity through LED (light emitting diode) circuits. Users can choose to test any pin/shell (test node) with a single push of a button, and any other nodes that are shorted to the test node, even if they are in the same connector, will light up with the test node.

The JPL-Cable Tester Boxes offers the following advantages:

1. Easy to use: The architecture is simple enough that it only takes 5 minutes for anyone to learn how operate the Cable Tester Box. No pre-pro-

gramming and calibration are required, since this box only checks continuity.

2. Fast: The cable tester box checks all the possible electrical connections in parallel at a push of a button. If a cable normally takes half an hour to test, using the Cable Tester Box will improve the speed to as little as 60 seconds to complete.

3. Versatile: Multiple cable tester boxes can be used together. As long as all the boxes share the same electrical potential, any number of connectors can be tested together.

This work was done by Jason H. Lee of Caltech for NASA's Jet Propulsion Laboratory. For more information, contact iaoffice@jpl.nasa.gov. NPO-46800

Programmable Oscillator

NASA's Jet Propulsion Laboratory, Pasadena, California

A programmable oscillator is a frequency synthesizer with an output phase that tracks an arbitrary function. An offset, phase-locked loop circuit is used in combination with an error control feedback loop to precisely control the output phase of the oscillator.

To down-convert the received signal, several stages of mixing may be employed with the compensation for the time-base distortion of the carrier occur-

ring at any one of those stages. In the Goldstone Solar System Radar (GSSR), the compensation occurs in the mixing from an intermediate frequency (IF), whose value is dependent on the station and band, to a common IF used in the final stage of down-conversion to baseband. The programmable oscillator (PO) is used in the final stage of down-conversion to generate the IF, along with a time-varying phase component that

matches the time-base distortion of the carrier, thus removing it from the final down-converted signal.

This work was done by Kevin J. Quirk, Ferze D. Patawaran, Danh H. Nguyen, and Clement G. Lee of Caltech and Huy Nguyen for NASA's Jet Propulsion Laboratory. Further information is contained in a TSP (see page 1). NPO-47657

Fault-Tolerant, Radiation-Hard DSP

This technology can be applied to commercial communications and GPS satellites.

Goddard Space Flight Center, Greenbelt, Maryland

Commercial digital signal processors (DSPs) for use in high-speed satellite computers are challenged by the damaging effects of space radiation, mainly single event upsets (SEUs) and single event functional interrupts (SEFIs). Innovations have been developed for mitigating the effects of SEUs and SEFIs, enabling the use of very-high-speed commercial DSPs with improved SEU tolerances. Time-triple modular redundancy (TTMR) is a method of applying traditional triple modular redun-

dancy on a single processor, exploiting the VLIW (very long instruction word) class of parallel processors. TTMR improves SEU rates substantially. SEFIs are solved by a SEFI-hardened core circuit, external to the microprocessor. It monitors the "health" of the processor, and if a SEFI occurs, forces the processor to return to performance through a series of escalating events.

TTMR and hardened-core solutions were developed for both DSPs and reconfigurable field-programmable gate

arrays (FPGAs). This includes advancement of TTMR algorithms for DSPs and reconfigurable FPGAs, plus a rad-hard, hardened-core integrated circuit that services both the DSP and FPGA. Additionally, a combined DSP and FPGA board architecture was fully developed into a rad-hard engineering product. This technology enables use of commercial off-the-shelf (COTS) DSPs in computers for satellite and other space applications, allowing rapid deployment at a much lower cost.

Traditional rad-hard space computers are very expensive and typically have long lead times. These computers are either based on traditional rad-hard processors, which have extremely low computational performance, or triple modular redundant (TMR) FPGA arrays, which suffer from power and complexity issues. Even more frustrating is that the TMR arrays of FPGAs require a fixed, external rad-hard voting element, thereby causing them to lose much of their reconfiguration capability and in some cases significant speed reduction.

The benefits of COTS high-performance signal processing include significant increase in onboard science data processing, enabling orders of magnitude reduction in required communication bandwidth for science data return, orders of magnitude improvement in onboard mission planning and critical decision making, and the ability to rapidly respond to changing mission environments, thus enabling opportunistic science and orders of magnitude reduction in the cost of mission operations through reduction of re-

quired staff. Additional benefits of COTS-based, high-performance signal processing include the ability to leverage considerable commercial and academic investments in advanced computing tools, techniques, and infrastructure, and the familiarity of the science and IT community with these computing environments.

This work was done by David Czajkowski of Space Micro, Inc. for Goddard Space Flight Center. Further information is contained in a TSP (see page 1). GSC-16078-1

Sub-Shot Noise Power Source for Microelectronics

Potential applications include microelectronics, sensors, and time/frequency standards.

NASA's Jet Propulsion Laboratory, Pasadena, California

Low-current, high-impedance microelectronic devices can be affected by electric current shot noise more than they are affected by Nyquist noise, even at room temperature. An approach to implementing a sub-shot noise current source for powering such devices is based on direct conversion of amplitude-squeezed light to photocurrent.

The phenomenon of optical squeezing allows for the optical measurements below the fundamental shot noise limit, which would be impossible in the domain of classical optics. This becomes possible by affecting the statistical properties of photons in an optical mode, which can be considered as a case of information encoding. Once encoded, the information describing the photon (or any other elementary excitations) statistics can be also transmitted. In fact, it is such information transduction from

optics to an electronics circuit, via photoelectric effect, that has allowed the observation of the optical squeezing. It is very difficult, if not technically impossible, to directly measure the statistical distribution of optical photons except at extremely low light level. The photoelectric current, on the other hand, can be easily analyzed using RF spectrum analyzers. Once it was observed that the photocurrent noise generated by a tested light source in question is below the shot noise limit (e.g. produced by a coherent light beam), it was concluded that the light source in question possess the property of amplitude squeezing.

The main novelty of this technology is to turn this well-known information transduction approach around. Instead of studying the statistical property of an optical mode by measuring the photoelectron statistics, an amplitude-squeezed light source and a high-effi-

ciency linear photodiode are used to generate photocurrent with sub-Poissonian electron statistics.

By powering microelectronic devices with this current source, their performance can be improved, especially their noise parameters. Therefore, a room-temperature sub-shot noise current source can be built that will be beneficial for a very broad range of low-power, low-noise electronic instruments and applications, both cryogenic and room-temperature. Taking advantage of recent demonstrations of the squeezed light sources based on optical micro-disks, this sub-shot noise current source can be made compatible with the size/power requirements specific of the electronic devices it will support.

This work was done by Dmitry V. Strekalov, Nan Yu, and Kamjou Mansour of Caltech for NASA's Jet Propulsion Laboratory. Further information is contained in a TSP (see page 1). NPO-47949



Asynchronous Message Service Reference Implementation

This software provides a library of middleware functions with a simple application programming interface, enabling implementation of distributed applications in conformance with the CCSDS AMS (Consultative Committee for Space Data Systems Asynchronous Message Service) specification.

The AMS service, and its protocols, implement an architectural concept under which the modules of mission systems may be designed as if they were to operate in isolation, each one producing and consuming mission information without explicit awareness of which other modules are currently operating. Communication relationships among such modules are self-configuring; this tends to minimize complexity in the development and operations of modular data systems.

A system built on this model is a “society” of generally autonomous, inter-operating modules that may fluctuate freely over time in response to changing mission objectives, modules’ functional upgrades, and recovery from individual module failure. The purpose of AMS, then, is to reduce mission cost and risk by providing standard, reusable infrastructure for the exchange of information among data system modules in a manner that is simple to use, highly automated, flexible, robust, scalable, and efficient.

The implementation is designed to spawn multiple threads of AMS functionality under the control of an AMS application program. These threads enable all members of an AMS-based, distributed application to discover one another in real time, subscribe to messages on specific topics, and to publish messages on specific topics. The query/reply (client/server) communication model is also supported.

Message exchange is optionally subject to encryption (to support confidentiality) and authorization. Fault tolerance measures in the discovery protocol minimize the likelihood of overall application failure due to any single operational error anywhere in the system. The multi-threaded design simplifies processing while enabling application

nodes to operate at high speeds; linked lists protected by mutex semaphores and condition variables are used for efficient, inter-thread communication. Applications may use a variety of transport protocols underlying AMS itself, including TCP (Transmission Control Protocol), UDP (User Datagram Protocol), and message queues.

This work was done by Scott C. Burleigh of Santa Barbara Applied Research for NASA’s Jet Propulsion Laboratory. Further information is contained in a TSP (see page 1). NPO-42814

This software is available for commercial licensing. Please contact Daniel Broderick of the California Institute of Technology at danielb@caltech.edu. Refer to NPO-42814.

Zero-Copy Objects System

Zero-Copy Objects System software enables application data to be encapsulated in layers of communication protocol without being copied. Indirect referencing enables application source data, either in memory or in a file, to be encapsulated “in place” within an unlimited number of protocol headers and/or trailers.

Zero-copy objects (ZCOs) are abstract data access representations designed to minimize I/O (input/output) in the encapsulation of application source data within one or more layers of communication protocol structure. They are constructed within the heap space of a “Simple Data Recorder” (SDR) data store to which all participating layers of the stack must have access. Each ZCO contains general information enabling access to the core source data object (an item of application data), together with (a) a linked list of zero or more specific “extents” that reference portions of this source data object, and (b) linked lists of protocol header and trailer capsules. The concatenation of the headers (in ascending stack sequence), the source data object extents, and the trailers (in descending stack sequence) constitute the transmitted data object constructed from the ZCO.

This scheme enables a source data object to be encapsulated in a succession of protocol layers without ever having to be copied from a buffer at one layer of the protocol stack to an encapsulating buffer at a lower layer of the stack. For

large source data objects, the savings in copy time and reduction in memory consumption may be considerable.

This work was done by Scott C. Burleigh of ACRO for NASA’s Jet Propulsion Laboratory. Further information is contained in a TSP (see page 1).

This software is available for commercial licensing. Please contact Daniel Broderick of the California Institute of Technology at danielb@caltech.edu. Refer to NPO-41627.

Delay and Disruption Tolerant Networking MACHETE Model

To verify satisfaction of communication requirements imposed by unique missions, as early as 2000, the Communications Networking Group at the Jet Propulsion Laboratory (JPL) saw the need for an environment to support interplanetary communication protocol design, validation, and characterization. JPL’s Multi-mission Advanced Communications Hybrid Environment for Test and Evaluation (MACHETE), described in “Simulator of Space Communication Networks” (NPO-41373) *NASA Tech Briefs*, Vol. 29, No. 8 (August 2005), p. 44, combines various commercial, non-commercial, and in-house custom tools for simulation and performance analysis of space networks. The MACHETE environment supports orbital analysis, link budget analysis, communications network simulations, and hardware-in-the-loop testing. As NASA is expanding its Space Communications and Navigation (SCaN) capabilities to support planned and future missions, building infrastructure to maintain services and developing enabling technologies, an important and broader role is seen for MACHETE in design-phase evaluation of future SCaN architectures.

To support evaluation of the developing Delay Tolerant Networking (DTN) field and its applicability for space networks, JPL developed MACHETE models for DTN – Bundle Protocol (BP) and Licklider/Long-haul Transmission Protocol (LTP). DTN is an Internet Research Task Force (IRTF) architecture providing communication in and/or through highly stressed networking environments such as space exploration and battlefield networks. Stressed networking environments include those

with intermittent (predictable and unknown) connectivity, large and/or variable delays, and high bit error rates. To provide its services over existing domain specific protocols, the DTN protocols reside at the application layer of the TCP/IP stack, forming a store-and-forward overlay network. The key capabilities of the Bundle Protocol include custody-based reliability, the ability to cope with intermittent connectivity, the ability to take advantage of scheduled and opportunistic connectivity, and late binding of names to addresses.

Internet standards are published in Request For Comments (RFCs), and the Bundle Protocol and LTP are described in RFC 5050 and RFC 5326, respectively. BP provides the store-carry-forward, custody transfer and naming capabilities of the DTN, while LTP was specifically developed for long-delay links. LTP allows for “red” and “green” data portions in a single session, where the red data portion uses retransmission and the green data portion does not. Unlike common Internet retransmission protocols, LTP adds the ability to suspend and resume timers when the link’s status changes. On occasion, the models are extended to include non-standard experimental features for validating project-specific performance or behavioral requirements. For instance, unlike standard simulation models, the BP model supports external traffic injection, which was used to verify correct behavior of the SharedNet middleware over DTN protocols and described at the SMC-IT 2006 conference (Second International Conference On Space Mission Challenges For Information Technology). The MACHETE LTP model supports all standard functions of LTP along with an optional priority-aware queuing system to prevent lower priority from blocking higher-priority traffic arriving later.

Furthermore, MACHETE contains Consultative Committee for Space Data Systems (CCSDS) protocol standards, such as Proximity-1, Advanced Orbiting Systems (AOS), Packet Telemetry/Telecommand, Space Communications Protocol Specification (SCPS), and the CCSDS File Delivery Protocol (CFDP). So, with the addition of DTN protocol libraries interplanetary network, engineers at JPL can characterize future space network performance trade-offs.

This work was done by John S. Seguí, Esther H. Jennings, and Jay L. Gao of Caltech for NASA’s Jet Propulsion Laboratory. For more information, contact iaoffice@jpl.nasa.gov.

This software is available for commercial licensing. Please contact Daniel Broderick of the California Institute of Technology at danielb@caltech.edu. Refer to NPO-43410.

Contact Graph Routing

Contact Graph Routing (CGR) is a dynamic routing system that computes routes through a time-varying topology of scheduled communication contacts in a network based on the DTN (Delay-Tolerant Networking) architecture. It is designed to enable dynamic selection of data transmission routes in a space network based on DTN. This dynamic responsiveness in route computation should be significantly more effective and less expensive than static routing, increasing total data return while at the same time reducing mission operations cost and risk.

The basic strategy of CGR is to take advantage of the fact that, since flight mission communication operations are planned in detail, the communication routes between any pair of “bundle agents” in a population of nodes that have all been informed of one another’s plans can be inferred from those plans rather than discovered via dialogue (which is impractical over long one-way-light-time space links). Messages that convey this planning information are used to construct “contact graphs” (time-varying models of network connectivity) from which CGR automatically computes efficient routes for bundles. Automatic route selection increases the flexibility and resilience of the space network, simplifying cross-support and reducing mission management costs.

Note that there are no “routing tables” in Contact Graph Routing. The best route for a bundle destined for a given node may routinely be different from the best route for a different bundle destined for the same node, depending on bundle priority, bundle expiration time, and changes in the current lengths of transmission queues for neighboring nodes; routes must be computed individually for each bundle, from the Bundle Protocol agent’s current network connectivity model for the bundle’s destination node (the contact graph). Clearly this places a premium on optimizing the implementation of the route computation algorithm. The scalability of CGR to very large networks remains a research topic.

The information carried by CGR contact plan messages is useful not only for dynamic route computation, but also for the implementation of rate control, con-

gestion forecasting, transmission episode initiation and termination, timeout interval computation, and retransmission timer suspension and resumption.

This work was done by Scott C. Burleigh of Caltech for NASA’s Jet Propulsion Laboratory. Further information is contained in a TSP (see page 1).

This software is available for commercial licensing. Please contact Daniel Broderick of the California Institute of Technology at danielb@caltech.edu. Refer to NPO-45488.

Parallel Eclipse Project Checkout

Parallel Eclipse Project Checkout (PEPC) is a program written to leverage parallelism and to automate the checkout process of plug-ins created in Eclipse RCP (Rich Client Platform). Eclipse plug-ins can be aggregated in a “feature project.” This innovation digests a feature description (xml file) and automatically checks out all of the plug-ins listed in the feature. This resolves the issue of manually checking out each plug-in required to work on the project. To minimize the amount of time necessary to checkout the plug-ins, this program makes the plug-in checkouts parallel. After parsing the feature, a request to checkout for each plug-in in the feature has been inserted. These requests are handled by a thread pool with a configurable number of threads. By checking out the plug-ins in parallel, the checkout process is streamlined before getting started on the project.

For instance, projects that took 30 minutes to checkout now take less than 5 minutes. The effect is especially clear on a Mac, which has a network monitor displaying the bandwidth use. When running the client from a developer’s home, the checkout process now saturates the bandwidth in order to get all the plug-ins checked out as fast as possible. For comparison, a checkout process that ranged from 8-200 Kbps from a developer’s home is now able to saturate a pipe of 1.3 Mbps, resulting in significantly faster checkouts.

Eclipse IDE (integrated development environment) tries to build a project as soon as it is downloaded. As part of another optimization, this innovation programmatically tells Eclipse to stop building while checkouts are happening, which dramatically reduces lock contention and enables plug-ins to continue downloading until all of them finish. Furthermore, the software re-enables

automatic building, and forces Eclipse to do a clean build once it finishes checking out all of the plug-ins.

This software is fully generic and does not contain any NASA-specific code. It can be applied to any Eclipse-based repository with a similar structure. It

also can apply build parameters and preferences automatically at the end of the checkout.

This work was done by Thomas M. Crockett, Joseph C. Joswig, Khawaja S. Shams and Mark W. Powell of Caltech and Andrew G. Bachmann of Stinger Ghaffarian Technolo-

gies Inc for NASA's Jet Propulsion Laboratory. For more information, contact iaoffice@jpl.nasa.gov.

This software is available for commercial licensing. Please contact Daniel Broderick of the California Institute of Technology at danielb@caltech.edu. Refer to NPO-47136.



Technique for Configuring an Actively Cooled Thermal Shield in a Flight System

New shields could potentially provide considerable mass savings.

Goddard Space Flight Center, Greenbelt, Maryland

Broad area cooling shields are a mass-efficient alternative to conductively cooled thermal radiation shielding. The shield would actively intercept a large portion of incident thermal radiation and transport the heat away using cryogenic helium gas. The design concept consists of a conductive and conformable surface that maximizes heat transfer and formability.

Broad Area Cooled (BAC) shields could potentially provide considerable mass savings for spaceflight applications by eliminating the need for a rigid thermal radiation shield for cryogen tanks. The BAC consists of a network of capillary tubes that are thermally connected to a conductive shield material. Chilled helium gas is circulated through the network and transports unwanted heat away from the cryogen tanks. The cryogenic helium gas is pumped and chilled simultaneously using a specialized pulse-tube cryocooler, which further improves the mass efficiency of the system. By reducing the thermal environment tempera-

ture from 300 to 100 K, the radiative heat load on a cryogen tank could be reduced by an order of magnitude. For a cryogenic liquid propellant scenario of oxygen and hydrogen, the boiloff of hydrogen would be significantly reduced and completely eliminated for oxygen.

A major challenge in implementing this technology on large tanks is that the BAC system must be easily scalable from lab demonstrations to full-scale missions. Also, the BAC shield must be conformable to complex shapes like spheres without losing the ability to maintain constant temperature throughout. The initial design maximizes thermal conductivity between the capillary tube and the conductive radiation shielding by using thin, corrugated aluminum foil with the tube running transverse to the folds. This configuration has the added benefit of enabling the foil to stretch and contract longitudinally. This allows the BAC to conform to the complex curvature of a cryogen tank, which is key to its success.

To demonstrate a BAC shield system with minimal impact to current cryogen tank designs, the shielding must be applied after the final assembly of the tank and supporting structure. One method is to pre-fabricate the shield in long strips. A spool of corrugated aluminum foil with a thermally sunk aluminum capillary running through the center could then be simply wound around the cryogen tanks and encapsulated within the multi-layer insulation (MLI) blanket. Then, on orbit, the BAC would intercept thermal radiation coming in through the MLI and transport it away from the cryogen tanks. An optimization of the design could be done to take into account mass savings from thinner MLI blankets, eliminating solid thermal shields, and ultimately, a reduction in the required cryogen tank size.

This work was done by Peter Barsknecht and Shuvo Mustafi of Goddard Space Flight Center. Further information is contained in a TSP (see page 1). GSC-15958-1



Use of Additives to Improve Performance of Methyl Butyrate-Based Lithium-Ion Electrolytes

A number of formulations are identified.

NASA's Jet Propulsion Laboratory, Pasadena, California

This work addresses the need for robust rechargeable batteries that can operate well over a wide temperature range. To this end, a number of electrolyte formulations have been developed that incorporate the use of electrolyte additives to improve the high-temperature resilience, low-temperature power capability, and life characteristics of methyl butyrate-based electrolyte solutions. These electrolyte additives include mono-fluoroethylene carbonate (FEC), lithium oxalate, vinylene carbonate (VC), and lithium bis(oxalato)borate (LiBOB), which have been shown to result in improved high-temperature resilience of all carbonate-based electrolytes.

Improved performance has been demonstrated of Li-ion cells with methyl butyrate-based electrolytes, including 1.20M LiPF₆ in EC+EMC+MB (20:20:60 v/v %); 1.20M LiPF₆ in EC+EMC+MB (20:20:60 v/v %) + 2% FEC; 1.20M LiPF₆ in EC+EMC+MB (20:20:60 v/v %) + 4% FEC; 1.20M LiPF₆ in EC+EMC+MB (20:20:60 v/v %) + lithium oxalate; 1.20M

LiPF₆ in EC+EMC+MB (20:20:60 v/v %) + 2% VC; and 1.20M LiPF₆ in EC+EMC+MB (20:20:60 v/v %) + 0.10M LiBOB. These electrolytes have been shown to improve performance in MCMB-LiNiCoO₂ and graphite-LiNi_{1/3}Co_{1/3}Mn_{1/3}O₂ experimental Li-ion cells.

A number of LiPF₆-based mixed carbonate electrolyte formulations have been developed that contain ester co-solvents, which have been optimized for operation at low temperature, while still providing reasonable performance at high temperature. For example, a number of ester co-solvents were investigated, including methyl propionate (MP), ethyl propionate (EP), methyl butyrate (MB), ethyl butyrate (EB), propyl butyrate (PB), and butyl butyrate (BB) in multi-component electrolytes of the following composition: 1.0M LiPF₆ in ethylene carbonate (EC) + ethyl methyl carbonate (EMC) + X (20:60:20 v/v %) [where X = ester co-solvent]. ["Optimized Carbonate and Ester-Based Li-Ion Electrolytes," *NASA Tech Briefs*, Vol. 32, No. 4 (April 2008), p. 56.] Focusing

upon improved rate capability at low temperatures (i.e., -20 to -40 °C), this approach was optimized further, resulting in the development of 1.20M LiPF₆ in EC+EMC+MP (20:20:60 v/v %) and 1.20M LiPF₆ in EC+EMC+EB (20:20:60 v/v %), which were demonstrated to operate well over a wide temperature range in MCMB-LiNiCoAlO₂ and Li₄Ti₅O₁₂-LiNiCoAlO₂ prototype cells

This work was done by Marshall C. Smart and Ratnakumar V. Bugga of Caltech for NASA's Jet Propulsion Laboratory. Further information is contained in a TSP (see page 1).

In accordance with Public Law 96-517, the contractor has elected to retain title to this invention. Inquiries concerning rights for its commercial use should be addressed to:

*Innovative Technology Assets Management
JPL*

Mail Stop 202-233

4800 Oak Grove Drive

Pasadena, CA 91109-8099

E-mail: iaoffice@jpl.nasa.gov

Refer to NPO-47537, volume and number of this NASA Tech Briefs issue, and the page number.

Li-Ion Cells Employing Electrolytes With Methyl Propionate and Ethyl Butyrate Co-Solvents

These electrolytes can be applied to hybrid electric vehicles that incorporate wide-operating-temperature-range cells.

NASA's Jet Propulsion Laboratory, Pasadena, California

Future NASA missions aimed at exploring Mars and the outer planets require rechargeable batteries that can operate at low temperatures to satisfy the requirements of such applications as landers, rovers, and penetrators. A number of terrestrial applications, such as hybrid electric vehicles (HEVs) and electric vehicles (EVs) also require energy storage devices that can operate over a wide temperature range (i.e., -40 to +70 °C), while still providing

high power capability and long life. Currently, the state-of-the-art lithium-ion system has been demonstrated to operate over a wide range of temperatures (-30 to +40 °C); however, the rate capability at the lower temperatures is very poor. These limitations at very low temperatures are due to poor electrolyte conductivity, poor lithium intercalation kinetics over the electrode surface layers, and poor ionic diffusion in the electrode bulk.

Two wide-operating-temperature-range electrolytes have been developed based on advances involving lithium hexafluorophosphate-based solutions in carbonate and carbonate + ester solvent blends, which have been further optimized in the context of the technology and targeted applications. The approaches employed include further optimization of electrolytes containing methyl propionate (MP) and ethyl butyrate (EB), which

are effective co-solvents, to widen the operating temperature range beyond the baseline systems. Attention was focused on further optimizing ester-based electrolyte formulations that have exhibited the best performance at temperatures ranging from -60 to +60 °C, with an emphasis upon improving the rate capability at -20 to -40 °C. This was accomplished by increasing electrolyte salt concentration to 1.20M and increasing the ester content to 60 percent by volume to increase the ionic conductivity at low temperatures.

Two JPL-developed electrolytes — 1.20M LiPF₆ in EC+EMC+MP (20:20:60

v/v %) and 1.20M LiPF₆ in EC+EMC+EB (20:20:60 v/v %) — operate effectively over a wide temperature range in MCMB-LiNiCoAlO₂ and Li₄Ti₅O₁₂-LiNiCoAlO₂ prototype cells. These electrolytes have enabled high rate performance at low temperature (i.e., up to 2.0C rates at -50 °C and 5.0C rates at -40 °C), and good cycling performance over a wide temperature range (i.e., from -40 to +70 °C). Current efforts are focused upon improving the high temperature resilience of the methyl propionate-based system through the use of electrolyte additives, which are envisioned to improve the nature of the solid electrolyte interphase (SEI) layers.

This work was done by Marshall C. Smart and Ratnakumar V. Bugga of Caltech for NASA's Jet Propulsion Laboratory. Further information is contained in a TSP (see page 1).

In accordance with Public Law 96-517, the contractor has elected to retain title to this invention. Inquiries concerning rights for its commercial use should be addressed to:

*Innovative Technology Assets Management
JPL*

Mail Stop 202-233

4800 Oak Grove Drive

Pasadena, CA 91109-8099

E-mail: iaoffice@jpl.nasa.gov

Refer to NPO-46976, volume and number of this NASA Tech Briefs issue, and the page number.



Improved Devices for Collecting Sweat for Chemical Analysis

Unlike prior devices, these would enable measurement of volumes of specimens.

Lyndon B. Johnson Space Center, Houston, Texas

Improved devices have been proposed for collecting sweat for biochemical analysis — especially for determination of the concentration of Ca^{2+} ions in sweat as a measure of loss of Ca from bones. Unlike commercially available sweat-collection patches used previously in monitoring osteoporosis and in qualitative screening for some drugs, the proposed devices would not allow evaporation of the volatile chemical components (mostly water) of sweat. Moreover, the proposed devices would be designed to enable determination of the volumes of collected sweat. From these volumes and the quantities of Ca^{2+} and/or other analytes as determined by other means summarized below, one could determine the concentrations of the analytes in sweat.

A device according to the proposal would be flexible and would be worn like a commercial sweat-collection patch. It would be made of molded polydimethylsiloxane (silicone rub-

ber) or other suitable material having properties that, for the purpose of analyzing sweat, are similar to those of glass. The die for molding the silicone rubber would be fabricated by a combination of lithography and electroplating. The die would reproducibly form, in the silicone rubber, a precisely defined number of capillary channels per unit area, each channel having a precisely defined volume. Optionally, electrodes for measuring the Ca^{2+} content of the sweat could be incorporated into the device.

The volume of sweat collected in the capillary channels of the device would be determined from (1) the amount of light or radio waves of a given wavelength absorbed by the device and (2) the known geometry of the array of capillary channels. Then, in one of two options, centrifugation would be performed to move the sweat from the capillary tubes to the region containing

the electrodes, which would be used to measure the Ca^{2+} content by a standard technique. In the other option, centrifugation would be performed to remove the sweat from the device to make the sweat available to other analytical instruments for measuring concentrations of substances other than Ca^{2+} .

This work was done by Daniel L. Feeback of Johnson Space Center and Mark S. F. Clarke of the University of Houston. Further information is contained in a TSP (see page 1).

In accordance with Public Law 96-517, the contractor has elected to retain title to this invention. Inquiries concerning rights for its commercial use should be addressed to:

*University of Houston
Department of Health and Human Performance
Laboratory of Integrated Physiology
3855 Holman St., Room 104 Garrison
Houston, TX 77201*

Refer to MSC-23625-1, volume and number of this NASA Tech Briefs issue, and the page number.

Tissue Photolithography

This method for extracting pure DNA from single cancer cells enables high-specificity cancer identification.

NASA's Jet Propulsion Laboratory, Pasadena, California

Tissue lithography will enable physicians and researchers to obtain macromolecules with high purity (>90 percent) from desired cells in conventionally processed, clinical tissues by simply annotating the desired cells on a computer screen. After identifying the desired cells, a suitable lithography mask will be generated to protect the contents of the desired cells while allowing destruction of all undesired cells by irradiation with ultraviolet light. The DNA from the protected cells can be used in a number of downstream applications including DNA sequencing. The purity (i.e., macromolecules isolated from specific cell types) of such specimens will greatly enhance the value and information of downstream applications.

In this method, the specific cells are isolated on a microscope slide using photolithography, which will be faster, more specific, and less expensive than current methods. It relies on the fact that many biological molecules such as DNA are photosensitive and can be destroyed by ultraviolet irradiation. Therefore, it is possible to “protect” the contents of desired cells, yet destroy undesired cells. This approach leverages the technologies of the microelectronics industry, which can make features smaller than 1 μm with photolithography.

A variety of ways has been created to achieve identification of the desired cell, and also to designate the other cells for destruction. This can be accomplished through chrome masks, direct laser writ-

ing, and also active masking using dynamic arrays. Image recognition is envisioned as one method for identifying cell nuclei and cell membranes. The pathologist can identify the cells of interest using a microscopic computerized image of the slide, and appropriate custom software.

In one of the approaches described in this work, the software converts the selection into a digital mask that can be fed into a direct laser writer, e.g. the Heidelberg DWL66. Such a machine uses a metalized glass plate (with chrome metallization) on which there is a thin layer of photoresist. The laser transfers the digital mask onto the photoresist by direct writing, with typical best resolution of 2 μm . The plate is

then developed to remove the exposed photoresist, which leaves the exposed areas susceptible to chemical chrome etch. The etch removes the unprotected chrome. The rest of the photoresist is then removed, by either ultraviolet organic solvent or overdevelopment. The remaining chrome pattern is quickly oxidized by atmospheric exposure (typically within 30 seconds).

The ready chrome mask is now applied to the tissue slide and aligned manually, or using automatic software and pre-de-

signed alignment marks. The slide plate sandwich is then exposed to UV to destroy the DNA of the unwanted cells. The slide and plate are separated and the slide is processed in a standard way to prepare for polymerase chain reaction (PCR) and potential identification of cancer sequences.

This work was done by Lawrence A. Wade of Caltech and Emil Kartalov, Darryl Shibata, and Clive Taylor of the University of Southern California for NASA's Jet Propulsion Laboratory. Further information is contained in a TSP (see page 1).

In accordance with Public Law 96-517, the contractor has elected to retain title to this invention. Inquiries concerning rights for its commercial use should be addressed to:

*Innovative Technology Assets Management
JPL*

*Mail Stop 202-233
4800 Oak Grove Drive
Pasadena, CA 91109-8099
E-mail: iaoffice@jpl.nasa.gov*

Refer to NPO-47507, volume and number of this NASA Tech Briefs issue, and the page number.

Method for Impeding Degradation of Porous Silicon Structures

This method tailors degradation of a drug delivery system to enable controlled release of therapeutic agents.

Lyndon B. Johnson Space Center, Houston, Texas

This invention relates to surface modification of porosified silicon (pSi) structures with poly(alkylene) glycols for the purpose of controlled degradation of the silicon matrix and tailored release of encapsulated substances for biomedical applications. The pSi structures are currently used in diverse biomedical applications including bio-molecular screening, optical bio-sensing, and drug delivery by means of injectable/orally administered carriers and implantable devices.

The size of the pores and the surface chemistry of the pSi structure can be controlled during the microfabrication process and thereafter. A fine regulation of the degradation kinetics of mesoporous silicon structures is of fundamental importance. Polyethylene glycols (PEGs) represent the major category of surface modifying agents used in classical drug delivery systems and in pharmaceutical dosage forms. PEGylation enables avoidance of RES uptake, thus prolonging circulation time of intravenously injectable nanovectors. PEG molecules demonstrate little toxicity and immunogenicity, and are cleared from the body through the urine (molecular weight,

MW<30 kDa) or in the feces (MW>30kDa).

The invention focuses on the possibility of finely tuning the degradation kinetics of the pSi nanovectors and other structures through surface conjugation of PEGs with various backbone lengths/MWs. To prove the concept, pSi nanovectors were covalently conjugated to seven PEGs with MW from 245 to 5,000 Da and their degradation kinetics in physiologically relevant media (phosphate buffer saline, PBS pH7.4, and fetal bovine serum) was assessed by the elemental analysis of the Si using inductive coupled plasma atomic emission spectroscopy (ICP-AES). The conjugation of the PEG with lowest MW to the nanovectors surface did not induce any change in the degradation kinetics in serum, but inhibited degradation and consequently the release of orthosilicic acid into buffer. When PEGs with the longer chains were evaluated, Si mass loss from the nanovectors was slowed down, and the PEGylated structures were almost fully degraded within 18–24 hours in serum and within 48 hours in PBS. The most dramatic effect was observed for high MW PEGs 3,400 and 5,000 Da, which prominently inhibited the degradation of

the systems, with complete degradation achieved only after four days. For these PEGs, during the early stages of the degradation, there was a “lag” period of little or no Si mass loss from the nanovector.

The obtained profiles were in agreement with the erosion of the nanovector surface as observed by scanning electron microscopy.

This work was done by Biana Godin Vientchouk and Mauro Ferrari of the University of Texas Health Science Center at Houston, Biomedical Engineering, for Johnson Space Center. For further information, contact the JSC Innovation Partnerships Office at (281) 483-3809.

In accordance with Public Law 96-517, the contractor has elected to retain title to this invention. Inquiries concerning rights for its commercial use should be addressed to:

*University of Texas
Health Science Center at Houston
The Office of Technology Management
UCT 720*

*Houston, TX 77030
Phone No.: (713) 500-3369*

E-mail: uthsch-otm@uth.tmc.edu

Refer to MSC-24566-1, volume and number of this NASA Tech Briefs issue, and the page number.

External Cooling Coupled to Reduced Extremity Pressure Device

The use of reduced-pressure boots and gloves may mitigate the effects of stroke and heart attacks.

Lyndon B. Johnson Space Center, Houston, Texas

Although suited astronauts are currently cooled with a Liquid Cooled Ventilation Garment (LCVG), which can remove up to 85 percent of body heat,

their effectiveness is limited because cooling must penetrate layers of skin, muscle, fat, bone, and tissue to reach the bloodstream, where its effect is promi-

nent. Vasoconstriction further reduces the effectiveness by limiting arterial flow when exposed to cold (the frostbite response), resulting in a time constant on

the order of 20 minutes from application to maximum effect. This delay can be crucial in severe exposure to hypo- or hyper-thermic conditions, compromising homeostasis.

The purpose of this innovation is to provide a lightweight, effective means of delivering heat or cold from an external source directly to the bloodstream. The effectiveness of this ECCREP (External Cooling Coupled to Reduced Extremity Pressure) device is based on not having to penetrate layers of skin, muscle, fat, and tissue, thereby avoiding the thermal lag associated with their mass and heat capacity. This is accomplished by means of an outer boot operating at a slightly reduced pressure than the rest of the body, combined with an inner boot cooled or heated by an external source via water or chemicals. Heat transfer from the external source to the foot takes place by means of circulating water or flexible heat pipes. The envisioned device, by applying its effect to only the foot or hand, has minimal power, flow, and mass requirements, making it attrac-

tive for the space/planetary operations environment and compatible with existing or modified extra-vehicular activity (EVA) suits, boots, and gloves.

In the glove configuration, the design may also have the added benefit of enhancing manual dexterity, a result of operating at a lower pressure than current EVA gloves. A boot configuration is preferable to a glove because the foot does not have any requirement for manual dexterity. The theoretical basis of the innovation is in the fact that heat transfer from the human body to its surroundings takes place largely in the extremities, especially the hands and feet. When exposed to heat, for example, large volumes of blood are directed to the hands and feet, which act as pin fin heat exchangers. This reaction is countermanded when extreme cold is applied to the skin to remove heat, as in the case of an LCVG, because extreme cold sets up vasoconstriction that limits bloodflow.

The theoretical basis of the innovation is that this countermand command

is apparently bypassed in the presence of reduced pressure. The ECCREP device accelerates blood pooling in the capillaries and arterioles of the hand or foot due to reduced pressure, then applies cold or heat through an external source to turn the limb into a "super heat exchanger."

The advantages of the device include the ability to deliver heat or cold more directly to the bloodstream, thus reducing the time lag of effectiveness; the ability to mitigate dehydration (sweat) and electrolyte loss; the potential to increase exercise performance and endurance (keys to operations in EVA and countermeasures while in orbit); and the possible mitigation of decrements in cognitive, motor, and immune system function associated with high-stress operations such as ascent, entry, and landing during long-duration and short-duration missions.

This work was done by Lawrence H. Kuznetz of Johnson Space Center. Further information is contained in a TSP (see page 1). MSC-23849-1



A Zero-Gravity Cup for Drinking Beverages in Microgravity

This spill-resistant cup can be used by commuters for general beverage consumption on-the-go.

Lyndon B. Johnson Space Center, Houston, Texas

To date, the method for astronauts to drink liquids in microgravity or weightless environments is to suck the liquid from a bag or pouch through a straw. A new beverage cup works in microgravity and allows astronauts to drink liquids from a cup in a manner consistent with that on Earth.

The cup is capable of holding beverages with an angled channel running along the wall from the bottom to the lip. In microgravity, a beverage is placed into the cup using the galley dispenser. The angled channel acts as an open passage that contains only two sides where capillary forces move the liquid along the channel until it reaches the top lip where the forces reach an equilibrium and the flow stops. When one sips the liquid at the lip of the channel, the capillary force equilibrium is upset and more liquid flows to the lip from the reservoir at the bottom to re-establish the equilibrium. This sipping process can continue until the total liquid contents of the cup is consumed, leaving only a few residual drops — about the same quantity as in a ceramic cup when it is drunk dry on Earth.

The free surface profile, governed by surface tension forces, was sufficient to keep the water from spilling during normal cup motions, thus allowing for the cup to be moved about like one would normally do for drinking beverages during a meal. Unlike on Earth, the cup could not be set on a table, but it could be parked on a wall and when desired, picked “up” for a sip.

Flexible walls functioning as a default handle proved to be a highly desirable feature. After the prototype cup was used with coffee where the remaining few drops were allowed to dry, the coffee residue as a contaminant altered the contact angle properties such that when refilled, the coffee was reluctant to move up the channel. A few gentle squeezes of the channel, reducing the angle to a value near zero degrees, increased the effect of capillary motion and quickly moved the coffee to the lip where thereafter the squeezing was unnecessary and



Figure 1. Astronaut Don Pettit Moves the 0 G Cup about the cabin without spillage while Steve Bowen takes a sip of tea.



Figure 2. Top View of the 0 G Cup showing the cup profile and the liquid channel at the rim.

the coffee could be sipped normally. As the cup begins to empty, again, gently squeezing the channel walls together, decreasing the angle to a near zero value, helps move the last few drops to the lip. Having a flexible channel is thus useful in initially priming of the fluid if the walls are contaminated from a prior

use and in drinking the last few drops.

The main body of the cup could be made from a material optimized for overall cup design, with a specialized coating applied to the inside region of the channel. An example would be a stainless steel cup with an enamel or ceramic coating applied to the inside of

the channel. Such a coating could have low contact angles, those closer to glass than metal or plastic, and not pose a breakage safety hazard.

This work was done by Donald R. Pettit of Johnson Space Center, Mark Weislogel of Port-

land State University, and Paul Concus and Robert Finn, independent consultants. For further information, contact the JSC Innovation Partnerships Office at (281) 483-3809.

This is the invention of a NASA employee, and a patent application has been filed. In-

quiries concerning license for its commercial development may be addressed to the inventor:

Donald R. Pettit

E-mail: mpillbox@sbcglobal.net

Refer to MSC-24558-1.

Co-Flow Hollow Cathode Technology

NASA's Jet Propulsion Laboratory, Pasadena, California

Hall thrusters utilize identical hollow cathode technology as ion thrusters, yet must operate at much higher mass flow rates in order to efficiently couple to the bulk plasma discharge. Higher flow rates are necessary in order to provide enough neutral collisions to transport electrons across magnetic fields so that they can reach the discharge. This higher flow rate, however, has potential life-limiting implications for the operation of the cathode.

A solution to the problem involves splitting the mass flow into the hollow cathode into two streams, the internal and external flows. The internal flow is fixed and set such that the neutral pres-

sure in the cathode allows for a high utilization of the emitter surface area. The external flow is variable depending on the flow rate through the anode of the Hall thruster, but also has a minimum in order to suppress high-energy ion generation.

In the co-flow hollow cathode, the cathode assembly is mounted on thruster centerline, inside the inner magnetic core of the thruster. An annular gas plenum is placed at the base of the cathode and propellant is fed throughout to produce an azimuthally symmetric flow of gas that evenly expands around the cathode keeper. This configuration maximizes propellant uti-

lization and is not subject to erosion processes.

External gas feeds have been considered in the past for ion thruster applications, but usually in the context of eliminating high energy ion production. This approach is adapted specifically for the Hall thruster and exploits the geometry of a Hall thruster to feed and focus the external flow without introducing significant new complexity to the thruster design.

This work was done by Richard R. Hofer and Dan M. Goebel of Caltech for NASA's Jet Propulsion Laboratory. Further information is contained in a TSP (see page 1). NPO-47901

Programmable Aperture With MEMS Microshutter Arrays

Goddard Space Flight Center, Greenbelt, Maryland

A microshutter array (MSA) has been developed for use as an aperture array for multi-object selections in James Webb Space Telescope (JWST) technology. Light shields, molybdenum nitride (MoN) coating on shutters, and aluminum/aluminum oxide coatings on interior walls are put on each shutter for light leak prevention, and to enhance optical contrast. Individual shutters are patterned with a torsion flexure that permits shutters to open 90° with a minimized mechanical stress concentration. The shutters are actuated magnetically, latched, and addressed electrostatically. Also, micromechanical features are tailored onto individual shutters to prevent stiction.

An individual shutter consists of a torsion hinge, a shutter blade, a front electrode that is coated on the shutter blade, a backside electrode that is coated on the interior walls, and a magnetic cobalt-iron coating. The magnetic coating is patterned into stripes on microshutters

so that shutters can respond to an external magnetic field for the magnetic actuation. A set of column electrodes is placed on top of shutters, and a set of row electrodes on sidewalls is underneath the shutters so that they can be electrostatically latched open.

A linear permanent magnet is aligned with the shutter rows and is positioned above a flipped upside-down array, and sweeps across the array in a direction parallel to shutter columns. As the magnet sweeps across the array, sequential rows of shutters are rotated from their natural horizontal orientation to a vertical open position, where they approach vertical electrodes on the sidewalls. When the electrodes are biased with a sufficient electrostatic force to overcome the mechanical restoring force of torsion bars, shutters remain latched to vertical electrodes in their open state. When the bias is removed, or is insufficient, the shutters return to their horizontal, closed positions. To release a

shutter, both the electrode on the shutter and the one on the back wall where the shutter sits are grounded. The shutters with one or both ungrounded electrodes are held open. Sub-micron bumps underneath light shields and silicon ribs on back walls are the two features to prevent stiction.

These features ensure that the microshutter array functions properly in mechanical motions. The MSA technology can be used primarily in multi-object imaging and spectroscopy, photomask generation, light switches, and in the stepper equipment used to make integrated circuits and MEMS (micro-electromechanical systems) devices.

This work was done by Samuel Moseley, Mary Li, and Alexander Kuttyrev of the University of Maryland, College Park; Gunther Kletetschka of the Catholic University of America; and Rainer Fettig of Raytheon Company for Goddard Space Flight Center. Further information is contained in a TSP (see page 1). GSC-15998-1

Polished Panel Optical Receiver for Simultaneous RF/Optical Telemetry With Large DSN Antennas

Three options are examined.

NASA's Jet Propulsion Laboratory, Pasadena, California

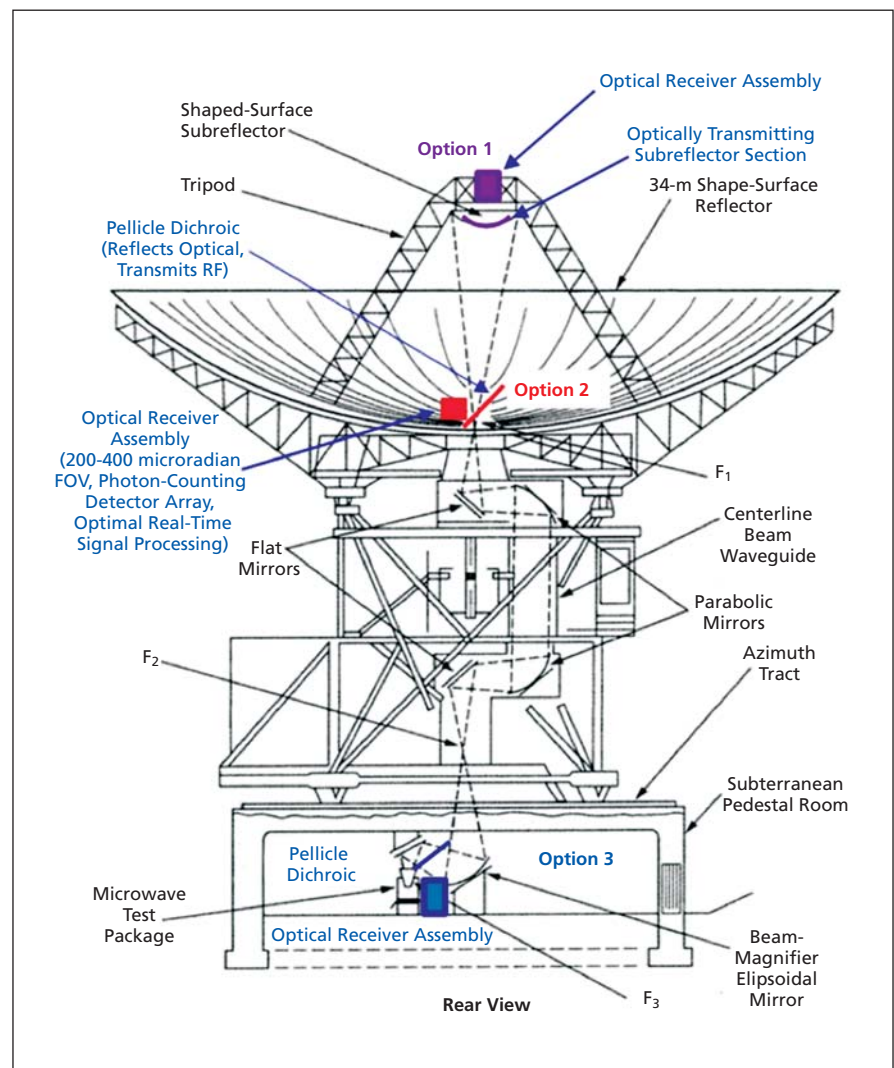
The “polished panel” optical receiver concept described here makes use of aluminum panels on the main reflector of the Deep Space Network’s (DSN’s) 34-meter antennas at optical wavelengths by polishing and coating their surface to efficiently reflect near-infrared wavelengths in the 1,064–1,550-nanometer range. Achievable surface smoothness is not a limiting factor for aluminum panels, and initial field experiments indicate that the surface quality of microwave aluminum panels is sufficient to concentrate the light into small, but not diffraction-limited, spots at their primary focus. Preliminary analysis of data from high-quality microwave panels has shown that the light can be concentrated into 200–400 microradian cones, resulting in spot diameters of 2–4 mm at the 10-meter primary focus F_0 shown in the figure, or 2–4 cm spots at F_1 after magnification by the subreflector, which results in an effective focal length of about 100 meters. Three distinct implementation options are possible, with theoretically identical tracking and communications performance:

Option 1: The communications assembly could be placed directly behind the subreflector at F_0 , but this placement would require replacing the existing all-aluminum subreflector with a new design that transmits optical wavelengths but reflects RF, thus transmitting the optical signal to the primary focus of the parabolic polished aluminum panels at F_0 , as shown in the figure. While this approach includes no design change to the subreflector shape, it does alter the RF performance by causing an increase in system noise temperature due to the imperfect nature of the RF reflectivity of the splitter coating. For example, one design point achieved for the splitter coating corresponds to approximately 90% RF reflection and 90% optical transmission. Use of this coating and its associate 10% leakage would cause an unacceptable increase in system temperature of approximately 30 K. Redesign of the coating is possible; however, any increase in RF reflectivity comes at the expense of reduced optical transmission. Appropriate use of this trade space in the context

of the polished panel concept is an area for future study. An advantage of this approach is that since the focal-spot is effectively at the prime focus of the panel (10 m), the spot-size will only be 2–4 mm at this location; hence, relatively small area photon-counting detector arrays could be employed.

Option 2: Alternately, the optical communications assembly could be located near the first available focal-spot F_1 following reflection by the subreflector (which would have to be polished), next to the input to the beam waveguide on the main reflector as shown in the figure. This placement requires an

RF/optical dichroic that reflects optical but transmits RF wavelengths, which can be implemented as a dielectric-coated pellicle, similar to commercial pellicle dichroics currently available in sufficiently large sizes. However, since this placement requires the pellicle to transmit large amounts of RF power in transmit mode, careful design will be required to ensure that the pellicle is not damaged due to absorption of RF energy during uplink transmission. Since the effective focal-length after subreflector magnification is about 100 m, the estimated spot-size at F_1 is 2–4 cm in diameter, requiring the develop-



Optical Communications Receiver Assembly, placed at F_0 (Option 1) and F_1 (Option 2) on a DSN 34-meter antenna.

ment of large-area photon-counting array detectors for best performance. However, the spot-size can be decreased by a factor of 3 to about 1 cm using commercially available optics, relaxing the requirements on the detector array to manageable proportions.

Option 3: Finally, the optical communications assembly could be placed inside the pedestal room, and separated from the RF signal after the ellipsoid and before the signal reached the microwave receiver via an RF/optical dichroic near F_3 , as shown in the figure. This placement would require polishing and coating the inner portions of all five mirrors of the beam waveguide (BWG) to very high optical reflectivity, but would have the advantage of protecting the optical communications assembly from the elements. If the mirrors could be polished to 95% reflectivity, then a loss of $0.95^5=0.77$ would occur to both the optical signal and the background, which is only about 1 dB and hence would not im-

pair communications performance significantly. However, this option is the most complicated to implement, requiring large-scale resurfacing of the BWG mirrors in addition to polishing the subreflector, hence it would likely incur the greatest cost.

For either approach, the reflected light is filtered using a narrowband optical filter to minimize background interference. At 1,550-nm wavelength, filter bandwidths of 2 Å are feasible, with high peak transmission (80%) suitable for communications applications. Detailed analyses of tracking and communication performance of a generic polished-panel optical receiver is presented in other papers where pulse-position modulation and photon-counting detection are assumed, and it is shown that typical mission requirements to Mars can be met using polished-panel optical receivers even when pointing close to the Sun. Note that since receiver performance depends on field-of-view rather than spot-size, the analysis presented in

these papers applies equally to both design options.

In addition to theoretical analyses, preliminary polished-panel experiments are underway at the Venus site (DSS-13), located at the Deep-Space Communications Complex in Goldstone, California. These experiments are designed to measure the actual spot-size of a polished DSN panel as well as a more precise polished ALMA panel originally designed for near THz (900 GHz) operation. The key concepts of closed-loop tracking using detector arrays, as well as precise measurement of communications parameters while tracking stars and bright planets simulating future deep-space laser sources, will be determined in a realistic field environment and evaluated to predict future deep-space communications performance.

This work was done by Victor A. Vilnrotter and Daniel J. Hoppe of Caltech for NASA's Jet Propulsion Laboratory. For more information, contact iaoffice@jpl.nasa.gov. NPO-47691



Adaptive System Modeling for Spacecraft Simulation

Lyndon B. Johnson Space Center, Houston, Texas

This invention introduces a methodology and associated software tools for automatically learning spacecraft system models without any assumptions regarding system behavior. Data stream mining techniques were used to learn models for critical portions of the International Space Station (ISS) Electrical Power System (EPS). Evaluation on historical ISS telemetry data shows that adaptive system modeling reduces simulation error anywhere from 50 to 90 percent over existing approaches.

The purpose of the methodology is to outline how someone can create ac-

curate system models from sensor (telemetry) data. The purpose of the software is to support the methodology. The software provides analysis tools to design the adaptive models. The software also provides the algorithms to initially build system models and continuously update them from the latest streaming sensor data. The main strengths are as follows:

- Creates accurate spacecraft system models without in-depth system knowledge or any assumptions about system behavior.

- Automatically updates/calibrates system models using the latest streaming sensor data.
- Creates device specific models that capture the exact behavior of devices of the same type.
- Adapts to evolving systems.
- Can reduce computational complexity (faster simulations).

This work was done by Justin Thomas of Johnson Space Center. For further information, contact the JSC Innovation Partnerships Office at (281) 483-3809. MSC-24419-1

Lidar-Based Navigation Algorithm for Safe Lunar Landing

This algorithm could be used as a sensor approach for navigation of autonomous air vehicles for military surveillance.

NASA's Jet Propulsion Laboratory, Pasadena, California

The purpose of Hazard Relative Navigation (HRN) is to provide measurements to the Navigation Filter so that it can limit errors on the position estimate after hazards have been detected. The hazards are detected by processing a hazard digital elevation map (HDEM). The HRN process takes lidar images as the spacecraft descends to the surface and matches these to the HDEM to compute relative position measurements. Since the HDEM has the hazards embedded in it, the position measurements are relative to the hazards, hence the name Hazard Relative Navigation.

HRN processing starts with an initial elevation map from the Hazard Detection and Avoidance (HDA) phase. This map is generated by mosaicking the lidar over the Hazard Map Area (HMA). A feature selector is applied to the map to find a reference surface point that is surrounded by significant terrain relief and is therefore easier to identify in subsequent lidar images. This reference point does not have to be the landing site, and it probably won't be because the landing site should be free of terrain relief.

Next, the gimbal points the lidar sensor at the reference point and a lidar image is taken. The lidar image is converted to 3D points and these points are transformed into the local level coordinate frame using the current knowledge of the spacecraft position and attitude. These points are re-gridded into an elevation map. This elevation map is spatially correlated with the HDEM to determine the position change of the reference point in the local level frame between where it was predicted to be given the current state and its observed position when the HDEM was constructed.

The reference point is not actually moving in the local level frame, so this change in position is actually a measurement of current navigation state error growth from the time the HDEM was created. Since attitude errors are expected to be very small, the change in position of the reference point is most likely due to errors in the position of the spacecraft. This process is repeated with multiple new lidar images as the spacecraft descends.

During descent, the correlation performance degrades due to the shrinking field of view, increasing resolution and

changing in view angle. The ground sample distance (GSD) of the basemap should be no more than twice the GSD of the current lidar map. To prevent the correlation from failing, resulting in a loss of knowledge of the position error on the reference point, a new base map is generated for correlation. This new base map is created by mosaicking the lidar around the landing site. A new, higher-resolution elevation map is created from the lidar mosaic. The feature selector is applied to the new base map to generate a new reference point. Lidar images are then taken of this new reference point and correlated with the new base map.

The process of generating a new base map, then correlating lidar images to it, is repeated until the beginning of vertical descent (30 m). Each time the base map changes, it is correlated with the previous base map to tie its position to the original HDEM. This correlation introduces a fixed error to the estimate of the change in position of the original reference point. Fortunately, this fixed error is a function of the resolution of the corresponding base map, so the fixed error contribution is decreasing.

The algorithm is related to other motion and velocity estimation algorithms, but is different because the data processed is 3D points, not camera images. This difference in input data makes a large difference in how feature selection and correlation are implemented. The algorithm also must handle oblique viewing angles and rel-

ative high sensor noise; both of these make HRN challenging. Finally the HRN algorithm actually commands the lidar to collect data during descent that is the best for HRN. This “Active Vision” approach was not used in previous work.

This work was done by David M. Myers, Andrew E. Johnson, and Robert A. Werner of

Caltech for NASA’s Jet Propulsion Laboratory. Further information is contained in a TSP (see page 1).

The software used in this innovation is available for commercial licensing. Please contact Daniel Broderick of the California Institute of Technology at danielb@caltech.edu. Refer to NPO-47115.

Tracking Object Existence From an Autonomous Patrol Vehicle

These techniques could be part of a mobile surveillance system attached to a ground vehicle, boat, or airplane.

NASA’s Jet Propulsion Laboratory, Pasadena, California

An autonomous vehicle patrols a large region, during which an algorithm receives measurements of detected potential objects within its sensor range. The goal of the algorithm is to track all objects in the region over time. This problem differs from traditional multi-target tracking scenarios because the region of interest is much larger than the sensor range and relies on the movement of the sensor through this region for coverage. The goal is to know whether anything has changed between visits to the same location. In particular, two kinds of “alert” conditions must be detected: (1) a previously detected object has disappeared and (2) a new object has appeared in a location already checked.

For the time an object is within sensor range, the object can be assumed to remain stationary, changing position only between visits. The problem is difficult because the upstream object detection processing is likely to make many errors, resulting in heavy clutter (false positives) and missed detections (false negatives), and because only noisy, bearings-only measurements are available. This work has three main goals:

(1) Associate incoming measurements with known objects or mark them as new objects or false positives, as ap-

propriate. For this, a multiple hypothesis tracker was adapted to this scenario.

(2) Localize the objects using multiple bearings-only measurements to provide estimates of global position (e.g., latitude and longitude). A nonlinear Kalman filter extension provides these 2D position estimates using the 1D measurements.

(3) Calculate the probability that a suspected object truly exists (in the estimated position), and determine whether alert conditions have been triggered (for new objects or disappeared objects). The concept of a “probability of existence” was created, and a new Bayesian method for updating this probability at each time step was developed.

A probabilistic multiple hypothesis approach is chosen because of its superiority in handling the uncertainty arising from errors in sensors and upstream processes. However, traditional target tracking methods typically assume a stationary detection volume of interest, whereas in this case, one must make adjustments for being able to see only a small portion of the region of interest and understand when an “alert” situation has occurred. To track object existence

inside and outside the vehicle’s sensor range, a probability of existence was defined for each hypothesized object, and this value was updated at every time step in a Bayesian manner based on expected characteristics of the sensor and object and whether that object has been detected in the most recent time step. Then, this value feeds into a sequential probability ratio test (SPRT) to determine the “status” of the object (suspected, confirmed, or deleted). Alerts are sent upon selected status transitions. Additionally, in order to track objects that move in and out of sensor range — and update the probability of existence appropriately — a variable “probability detection” has been defined and the hypothesis probability equations have been re-derived to accommodate this change.

Unsupervised object tracking is a pervasive issue in automated perception systems. This work could apply to any mobile platform (ground vehicle, sea vessel, air vehicle, or orbiter) that intermittently revisits regions of interest and needs to determine whether anything interesting has changed.

This work was done by Michael Wolf and Lucas Scharenbroich of Caltech for NASA’s Jet Propulsion Laboratory. For more information, contact iaoffice@jpl.nasa.gov. NPO-47274



Books & Reports

Rad-Hard, Miniaturized, Scalable, High-Voltage Switching Module for Power Applications

A paper discusses the successful development of a miniaturized radiation hardened high-voltage switching module operating at 2.5 kV suitable for space application. The high-voltage architecture was designed, fabricated, and tested using a commercial process that uses a unique combination of 0.25 μm CMOS (complementary metal oxide semiconductor) transistors and high-voltage lateral DMOS (diffusion metal oxide semiconductor) device with high breakdown voltage (>650 V). The high-voltage requirements are achieved by stacking a number of DMOS devices within one module, while two modules can be placed in series to achieve higher voltages.

Besides the high-voltage requirements, a second generation prototype is currently being developed to provide improved switching capabilities (rise time and fall time for full range of target voltages and currents), the ability to scale the output voltage to a desired value with good accuracy (few percent) up to 10 kV, to cover a wide range of high-voltage applications. In addition, to ensure miniaturization, long life, and high reliability, the assemblies will require intensive high-voltage electrostatic modeling (opti-

mized E-field distribution throughout the module) to complete the proposed packaging approach and test the applicability of using advanced materials in a space-like environment (temperature and pressure) to help prevent potential arcing and corona due to high field regions.

Finally, a single-event effect evaluation would have to be performed and single-event mitigation methods implemented at the design and system level or developed to ensure complete radiation hardness of the module.

This work was done by Philippe C. Adell, Mohammad Mojarradi, Linda Y. Del Castillo, and Tuan A. Vo of Caltech for NASA's Jet Propulsion Laboratory. Further information is contained in a TSP (see page 1). NPO-47784

Architecture for a 1-GHz Digital RADAR

An architecture for a Direct RF-digitization Type Digital Mode RADAR was developed at GSFC in 2008. Two variations of a basic architecture were developed for use on RADAR imaging missions using aircraft and spacecraft. Both systems can operate with a pulse repetition rate up to 10 MHz with 8 received RF samples per pulse repetition interval, or at up to 19 kHz with 4K received RF samples per pulse repetition interval.

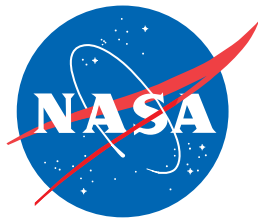
The first design describes a computer architecture for a Continuous Mode RADAR transceiver with a real-time sig-

nal processing and display architecture. The architecture can operate at a high pulse repetition rate without interruption for an infinite amount of time. The second design describes a smaller and less costly burst mode RADAR that can transceive high pulse repetition rate RF signals without interruption for up to 37 seconds. The burst-mode RADAR was designed to operate on an off-line signal processing paradigm.

The temporal distribution of RF samples acquired and reported to the RADAR processor remains uniform and free of distortion in both proposed architectures. The majority of the RADAR's electronics is implemented in digital CMOS (complementary metal oxide semiconductor), and analog circuits are restricted to signal amplification operations and analog to digital conversion.

An implementation of the proposed systems will create a 1-GHz, Direct RF-digitization Type, L-Band Digital RADAR — the highest band achievable for Nyquist Rate, Direct RF-digitization Systems that do not implement an electronic IF downsample stage (after the receiver signal amplification stage), using commercially available off-the-shelf integrated circuits.

This work was done by Udayan Mallik at Goddard Space Flight Center. Further information is contained in a TSP (see page 1). GSC-15716-1



National Aeronautics and
Space Administration